Colloids and Surfaces B: Biointerfaces 222 (2023) 113136

Contents lists available at ScienceDirect

Colloids and Surfaces B: Biointerfaces

journal homepage: www.elsevier.com/locate/colsurfb

Surface characterization of alkane viral anchoring films prepared by titanate-assisted organosilanization

Aida Sanz Calderón [a], Miguel Cantero [b], Uxia Pérez [c,f], Paula Ortega-González [c], Carmen San Martín [c], Pedro. J. de Pablo [b,d], Miguel Manso Silván [a,*], Mercedes Hernando-Pérez [e,*]

[a] Department of Applied Physics, Centro de Microanálisis de Materiales, and Instituto de Ciencia de Materiales Nicolás Cabrera, Universidad Autónoma de Madrid, Ciudad Universitaria de Cantoblanco, 28049 Madrid, Spain
[b] Department of Condensed Matter Physics and Instituto de Ciencia de Materiales Nicolás Cabrera, Universidad Autónoma de Madrid, Ciudad Universitaria de Cantoblanco, 28049 Madrid, Spain
[c] Department of Macromolecular Structures, Centro Nacional de Biotecnología (CNB-CSIC), 28049 Madrid, Spain
[d] Instituto de Física de la Materia Condensada (IFIMAC), Universidad Autónoma de Madrid, Ciudad Universitaria de Cantoblanco, 28049 Madrid, Spain
[e] Department of Materials Physics and Instituto de Ciencia de Materiales Nicolás Cabrera, Universidad Autónoma de Madrid, Ciudad Universitaria de Cantoblanco, 28049 Madrid, Spain
[f] Department of Crystallography and Structural Biology, Instituto de Química Física Rocasolano, CSIC, 28006 Madrid, Spain

ARTICLE INFO

Keywords:
Hydrophobic surfaces
Titanate-assisted organosilanization
AFM
reovirus
human adenovirus

ABSTRACT

Studies of virus adsorption on surfaces with optimized properties have attracted a lot of interest, mainly due to the influence of the surface in the retention, orientation and stability of the viral capsids. Besides, viruses in whole or in parts can be used as cages or vectors in different areas, such as biomedicine and materials science. A key requirement for virus nanocage application is their physical properties, i.e. their mechanical response and the distribution of surface charge, which determine virus-substrate interactions and stability. In the present work we show two examples of viruses exhibiting strong surface interactions on homogeneous hydrophobic surfaces. The surfaces were prepared by titanate assisted organosilanization, a sol-gel spin coating process, followed by a mild annealing step. We show by surface and interface spectroscopies that the process allows trapping triethoxy-octylsilane (OCTS) molecules, exhibiting a hydrophobic alkane rich surface finishing. Furthermore, the surfaces remain flat and behave as more efficient sorptive surfaces for virus particles than mica or graphite (HOPG). Also, we determine by atomic force microscopy (AFM) the mechanical properties of two types of viruses (human adenovirus and reovirus) and compare the results obtained on the OCTS functionalized surfaces with those obtained on mica and HOPG. Finally, the TIPT+OCTS surfaces were validated as platforms for the morphological and mechanical characterization of virus particles by using adenovirus as initial model and using HOPG and mica as standard control surfaces. Then, the same characteristics were determined on reovirus using TIPT+OCTS and HOPG, as an original contribution to the catalogue of physical properties of viral particles.

1. Introduction

Viruses are infectious agents mainly composed of nucleic acids, either deoxyribonucleic (DNA) or ribonucleic acid (RNA), and shell called capsid [1]. In particular cases, viruses present more than one capsid and/or lipidic membranes (envelopes). The capsid plays a fundamental role, recognizing the host cell and anchoring to its membrane in order to penetrate and trigger the virus replication.

Although some viruses are the cause of human-concerning diseases, we can use them for beneficial purposes in various areas, such as in nanomedicine (vaccine vectors [2–4], drug delivery systems [5] and as template for nanoscale electronic components [6–8]). The uses of viruses in these different applications are due to some of their excellent characteristics, such as their structure, symmetry, and self- assembling ability [9].

These applications, and others, such as the development of antiviral/virucidal films [10], require knowledge of virus physical properties, and in particular, the virus-substrate interaction. Adhesion depends on the

* Corresponding authors.
E-mail addresses: miguel.manso@uam.es (M. Manso Silván), mercedes.hernando@uam.es (M. Hernando-Pérez).

https://doi.org/10.1016/j.colsurfb.2023.113136
Received 1 November 2022; Received in revised form 26 December 2022; Accepted 6 January 2023
Available online 10 January 2023

nature of the virus particle and on surface characteristics, such as roughness and surface chemistry [11,12]. The roughness difference between two objects determines their adhesion force [13]. Following JKR theory [14] and considering the diameter of the virus (R_V) and surface local radius (R_{sub}), the adhesion force ($F_{adhesion}$) is approximately proportional to the effective radius (R_{eff}), where $\frac{1}{R_{eff}} = \frac{1}{R_V} + \frac{1}{R_{sub}}$ is maximum when the surface is flat (R_{sub} tends to infinity) and minimum when the surface asperities are below the virus size ($R_{sub} << R_V$).

Topographic features on the substrate induce capillarity effects and chemical queues bring inhomogeneous surface charge, which leads to a modified virus-surface interaction [12,15]. Roughness leads to a redistribution of charges associated to the surface chemical groups and the surrounding ions according to the double layer model, thus altering the Gibbs energy of interaction (i.e. surface free energy or surface tension) [16]. However, several studies have confirmed high viral particle physisorption on hydrophobic materials [17–19]. All this suggests the deep interest in the thermodynamic analysis of the surfaces by using calorimetry [20] and appropriate models to derive predictive parameters (such as the Flory-Huggins parameter) allowing to estimate adhesive or non-adhesive regimes for colloidal structures such as microbial organisms [21].

The Sol-Gel method is a simple and low-cost technique that allows obtaining homogeneous thin films with a high control over the surface stoichiometry [22]. The process can be used to functionalize surfaces with organosilanes allowing protocols such as on-surface DNA hybridization [23]. In the precise framework of titanate assisted organo-silanization (TAOS), the process has been proven effective to produce surfaces with different dominant components of the surface tension: dispersive (hydrophobic), polar acid and polar basic [19]. The slower reactivity of the organosilane molecules within a titanate network makes them segregate towards the surface, leading to an effective exposure of the functional queues to the surface [24].

Among the group of viruses attracting most scientific and technological attention, human adenoviruses (*Adenoviridae* family) are pathogens associated to digestive infections, respiratory diseases and conjunctivitis. Adenoviruses have an icosahedral 90 nm diameter capsid that contains the dsDNA genome [25,26]. It is used in nanomedicine as a vector [27], as in the AstraZeneca and Janssen vaccines against SARS-CoV-2 [28], and also for the delivery of antitumor therapeutic agents [29]. Development of new applications of this virus justifies the need for an accurate determination of its mechanical properties [30] and adherence to surfaces. With analogue relevance, the human reovirus (Reoviridae family) can cause mild respiratory and gastrointestinal infections [31] and has been involved in the celiac disease [32]. Human reovirus has an icosahedral capsid of ~80 nm diameter, a double shell of proteins and a genome comprised of double-stranded RNA [33]. It is used in therapies against a wide variety of tumors due to its strong ability to effectively kill cancer cells.

In this work, Triethoxy-Octylsilane (OCTS) surfaces were prepared from an isopropyl orthotitanate sol to take advantage of the hydrophobic character exhibited by densely packed alkane surfaces[34,35]. Two different viruses of medical relevance, human adenovirus type 5 (Ad5) and human reovirus, were adsorbed on OCTS surfaces to characterize mechanical properties such as deformability, elasticity or breakage of the viral capsid [36–38]. We have carried out nanoindentation experiments by using atomic force microscopy (AFM) [38–40]. AFM allows obtaining nanometric resolution images of the structure of the viruses and studying their mechanical properties in physiological state.

The state of the art in the preparation and applications of TAO surfaces on the one hand, and the potential of the AFM to estimate the mechanical properties of viruses on the second hand, have served as the bases to state the main hypothesis justifying this work. That is, that the potential for retention and stability of viruses adsorbed on hydrophobic TAO surfaces could set the conditions for an optimized analysis of the mechanical properties of viruses using AFM.

2. Materials and methods

2.1. Preparation of hydrophobic surfaces

The deposition of hydrophobic TAOS thin films was carried out by Sol-Gel spin coating as illustrated in Supporting Information Fig. S1. For this purpose, a 0.4 M solution of isopropyl orthotinate (TIPT) with pH 1.2 adapted with HCl (0.1 M) was mixed in 1:1 vol ratio with different concentrations (0.1 M, 0.04 M or 0.01 M) of OCTS diluted in isopropanol. Prior to deposition, silicon wafers were cut using a diamond tip and washed with isopropanol. 50 μl of the resulting hybrid solutions were deposited on (100) silicon substrates of 1 cm^2 by spin coating using the spin coater Laurell WS-650MZ-23NPP equipment at 3000 rpm for 15 s. Forty replicates of films were made with different TIPT/OCTS concentration. Some of the replicas were used as spin coated, while others were annealed at 75ºC for 5 min to study the effect of soft annealing on organosilane relaxation.

2.2. Silanized surface characterization

We have used Fourier Transformed Infrared Spectroscopy (FTIR) to characterize the molecular structure of the films. Double sided intrinsic Si substrates were used for this characterization performed in transmission mode. FTIR spectra were acquired on a Cary 630 FTIR spectrometer in the range from 650 to 4000 cm^{-1}.

The study of the chemical composition of the surfaces was determined by means of X-ray photoelectron spectroscopy (XPS) using a PHOIBOS 150 9MCD analyzer (SPECS, Germany). The resulting spectra were obtained by irradiating with a non-monochromatic Al K_α source and an energy pass of 75 eV for the elemental scanning spectra and 25 eV for the higher resolution spectra. The obtained spectra were analyzed using Casa XPS software.

Rutherford backscattering spectrometry (RBS) was used to determine the in-depth chemical composition of the samples. The spectra were obtained with a Cockcroft-Walton tandem accelerator. The He ion beam has an incident energy of 2 MeV and an angle of incidence of 170º. The resulting spectra were analyzed with SIMNRA software [41].

The functional characterization of the surfaces was performed by measuring the static water contact angle (θ). We deposited four 70 μl drops of milliQ water on each surface using a KSV cam 101 goniometer. Contact angle values were calculated using KSV cam 2008 image analysis using Laplace-Young model.

The topography of the functionalized surfaces was characterized by AFM. A Nanotec Electrónica S.L. (Dulcinea) microscope was used, operating in dynamic mode using rectangular cantilevers (Olympus RC-800) with a nominal spring constant of 0.7 N/m.

2.3. Purification and preparation of viruses for AFM

For Ad5 virions, we have used the constructs Ad5/attP [42], and propagated at 37 ºC in HEK293 cells and harvested at 36 h post-infection. Ad5 viral particles were purified by centrifugation at 18 °C and 217,485 g in a 1.25–1.40 g/ml CsCl step gradient (90 min), followed by a 1.31 g/ml isopycnic one (18 h). CsCl solutions were prepared in TD1X buffer (0.137 M NaCl, 0.051 M KCl, 0.007 M Na_2HPO_4, 0.025 M Tris-HCl, pH 7.4). Bands extracted from the gradients were desalted on a Bio-Rad 10 DC column and stored in HBS buffer (0.02 M HEPES pH 7.8, 0.15 M NaCl) supplemented with 10% glycerol at − 80 °C until further use. The concentration of the viral particles of Ad5 was in the order of 5 ×E11 vp/ml.

Reovirus was propagated in L929 cells and purified from cell lysates using CsCl gradient centrifugation as described [43]. Reovirus particle concentration was estimated by spectral absorbance of purified virus at 260 nm (optical density at 260 nm [OD260] of 1 for 2.1 ×E12

particles/ml [44]) reaching 5.72 ×E13. Once the viruses were purified, they were diluted in the buffer. For adenovirus, HBS (0.02M HEPES, pH 7.8, 0.15 M NaCl) was used in a 3:40 ratio, and for reovirus TBS (0.15 M NaCl, 0.015 M $MgCl_2$ y 0.01 M Tris pH 7,4) in a 1:1000 ratio. For AFM experiments, a 40 μl volume of virus solution was incubated on the surface for 20 min at room temperature. The sample was then washed 5 times with the buffered saline solution to remove virus particles that had not been adsorbed on the surface and may hinder scanning. The AFM tip was pre wetted with approximately 30 μl of the saline solution used in each case to avoid bending the cantilever.

2.4. Virus particle adsorption and mechanical characterization

To determine the influence of the surface on the physical properties of viruses, we used AFM in physiological (liquid) conditions. AFM in liquid media has made possible not only the topographic characterization of individual virus particles under physiological conditions with a resolution of a few nanometers, but also has provided relevant information about their physical properties: elasticity, fragility, mechanical stability, or internal pressure of the capsid, and even their effective electrostatic charge [39,45–48].

We used conventional surfaces, including cleaved mica and highly oriented pyrolytic graphite (HOPG), to compare with our results on the TIPT+OCTS surface. Ad5 was adsorbed on functionalized mica in presence of nickel chloride by adding 5 mM $NiCl_2$ to the buffer as described in literature [46,49]. A 40 μl drop of virus solution described above is deposited on the surface of interest and characterized by AFM. For the study of mechanical properties, nanoindentation experiments are performed on single virus particles. We have used the jumping mode plus [50] to avoid the lateral forces induced by the cantilever lateral scanning and rectangular cantilevers (Olympus RC-800) with nominal spring constants of 0.1 N/m and 0.05 N/m. For the nanoindentation experiments an image of the virus is recorded to check the integrity of the structure and locate the center of the shell. Then, the AFM tip is moved on the top of the particle and a force−distance curve recorded at a loading rate of 150 nm/s. The images (128 × 128 pixels) and curves obtained are analyzed using WSxM 5.0 software [51].

3. Results

3.1. Physical chemistry of the OCTS surfaces

To assess the properties of OCTS surfaces with different processing history regarding their application as hydrophobic support for virus adsorption, we performed spectroscopic, microscopic, and functional analyses. We first optimized the OCTS content by a spectroscopic analysis using vibrational, interface and surface spectroscopies.

The FTIR spectra confirmed the presence of the expected molecular structures on each surface with a common pattern dominated by TIPT bands (Supporting Information, Fig. S2) at the lowest wavenumbers. We can observe a pronounced peak present in at approximately 1110 cm^{-1}, which corresponds to a silica layer on the Si substrate as deduced from the narrow shape of the band [52]. Relevantly, the doublet at around 2750–3000 cm^{-1}, clearly observable in the spectrum form the sample with higher concentration of OCTS, is a clear indication of the presence of integrated alkane structures [53] (note the dotted line circle around the described doublet in Fig. S2, top spectrum).

In order to perform an interface analysis of the TIPT+OCTS samples we carried out an RBS experiment. In the RBS spectrum for the TIPT sample (Fig. S3A), the first region at circa 600–700 keV, corresponds to the backscattered ions upon collision with oxygen. The deep edge at circa 1000 keV relates to the Si Substrate. The shoulder contribution at circa 1050–1200 keV corresponds to Cl, which remains as a byproduct of the condensation of TIPT sol. Finally, the wide peak centered at 1300 keV is related to the Ti contribution. In the case of the OCTS functionalized sample (Fig. S3B) the spectrum is similar, but two additional regions appear: the first one, a diffused shoulder corresponding to carbon at 500 keV, and the second one at energies of circa 1050 keV related to Si atoms on the surface of the sample. From the SIMNRA simulations of the two films we could confirm the slight difference in the estimated film thickness (with values of 79.6 nm for the pure TIPT film and 53.8 nm for the TIPT+OCTS film) and an estimation of C content on the surface, representing a 0.07% (excluding H).

To provide further detail of the surface chemistry, we performed an additional XPS analysis providing averaged stoichiometric information in a depth of less than 10 nm. Fig. 1 shows the XPS spectra obtained from the OCTS surfaces functionalized with 0.04 M concentration in comparison with the spectrum for TIPT. The quantification from the main core level contributions in the survey spectra of both surfaces reflects a 10 at% Ti for the OCTS sample (Fig. 1A) and a 14.2 at% for the TIPT sample (Fig. 1B). The difference in the atomic percentage suggests a screening of Ti composition of the OCTS sample by a surface layer. The presence of this additional top-layer can be confirmed by the presence of a Si 2p core level contribution on the OCTS functionalized surface representing a 5 at% (note the circle highlighting the absence of this peak in the TIPT sample on the top spectrum of Fig. 1A). Finally, additional illustrative evidence of the functionalization is the difference in the C 1 s surface stoichiometry estimated in 44 at% for the OCTS surface and 38 at% for the pure TIPT sample.

We additionally carried out an analysis of the C 1 s core level contributions. The area under the curve of the different contributions provides a quantitative estimation of the different C bond chemistry on the sample surface. From lower to higher binding energy, we can identify four contributions: C-H bonds at 284.5 eV, C-O-C and C-OH at 286.0 eV, C═O at 288.0 eV and O-C═O at 289.0 eV. To underline the differences between both samples, we show that the ratio between the C-O and C-H contributions is 0.16 for OCTS functionalized surface (Fig. 1C), but 0.25 for the TIPT surfaces (Fig. 1B).

3.2. Functional characterization of the OCTS substrate

The hydrophobic behavior of the surfaces was analyzed by measuring water contact angles in the sessile drop mode. For samples grown without further annealing, (Fig. S4A) an increasing trend of the contact angle is seen as the OCTS concentration is increased. This is due to the increased presence of C-H groups, which induce on the surface a hydrophobic character [54]. This increasing trend of the contact angle as a function of silane concentration is also observed in the softly annealed samples (Fig. S4B). The annealing induces an increase of their contact angle with respect to the room temperature samples, i.e., it emphasizes the hydrophobic character.

These results indicate that the most hydrophobic surfaces correspond to the highest concentration of silane (0.1 M OCTS). For this concentration, we obtain a contact angle value of 92 ± 1° for pristine OCTS surfaces, and 99 ± 1° for annealed surfaces. For the sake of comparison, the control sample (HOPG) has a contact angle of ~86° [55]. Therefore, the surfaces with higher OCTS concentration and annealing are the ones selected to perform the next virus adsorption studies, since the physisorption of viruses is pointed out in literature as enhanced on these surfaces [56,57].

To acquire high-quality images of virus particles in AFM it is key to work on flat substrates. Therefore, we characterized the topography of the functionalized surfaces by AFM. The maximum roughness (Rt) is the vertical distance between the highest and lowest peak. Root Mean Square (RMS) height is the square root of the pixel height distribution for the surface. (Fig. S5).

By performing an analytical study on the adsorption of viral particles of Ad5 and reovirus (Fig S6) on the different surfaces (Fig. S7), we found that the uptake of Ad5 particles on TIPT+OCTS is 5.0 ± 0.5 virus/μm^2 (N = 15) while on HOPG the uptake is 2.7 ± 0.3 virus/μm^2 (N = 15) and 4.2 ± 0.6 virus/μm^2 (N = 3) for mica in presence of nickel chloride. In the case of reovirus, we got an uptake of 6 ± 1 (N = 4) virus/μm^2 in

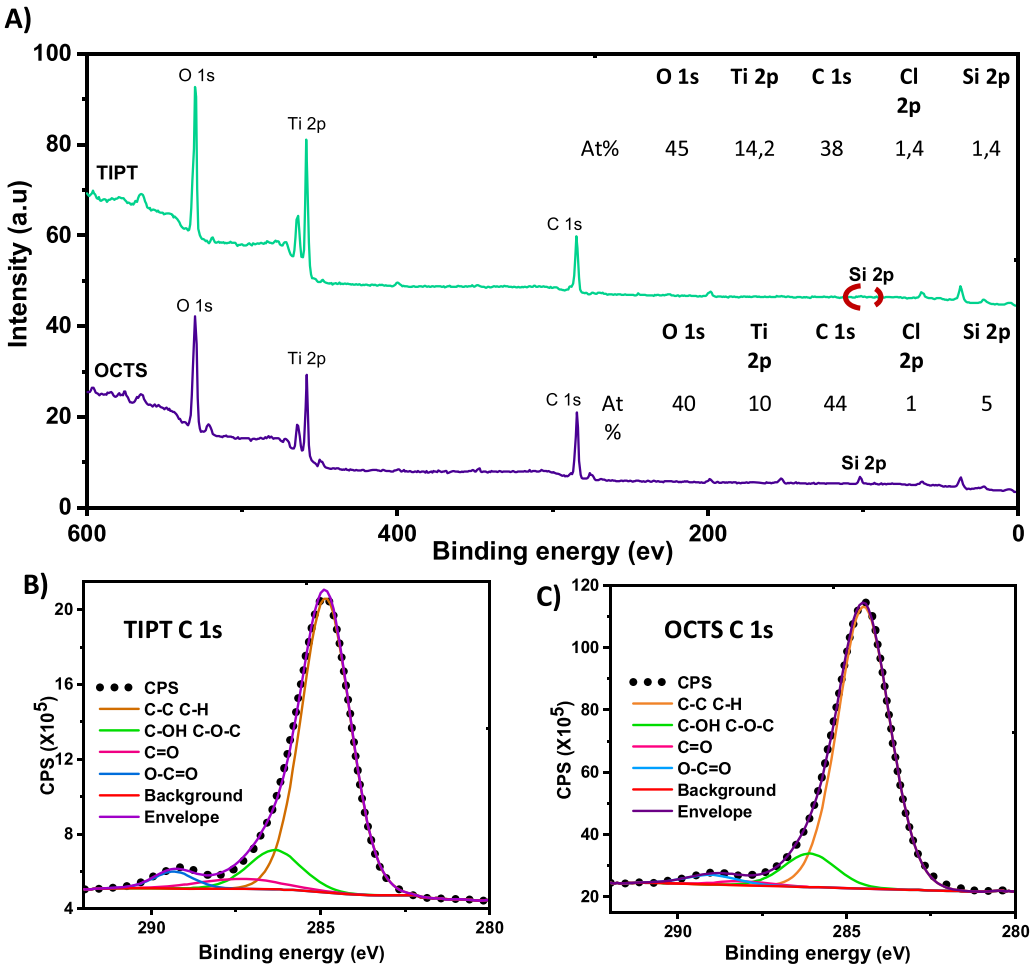

Fig. 1. XPS Spectra of surfaces. A) XPS Survey spectra of the OCTS functionalized and pure TIPT samples (the red mark indicates the absence of Si 2p in the TIPT sample). B) and C) C 1 s core level spectra of the OCTS and TIPT samples, respectively. The various curves show the contribution of the different C chemistry to the C1s spectrum.

TIPT+OCTS and 1.6 ± 0.7 virus/μm^2 (N = 4) on HOPG. Therefore, we observed for both viruses that more particles are adhered on functionalized surfaces compared to HOPG (Fig. S7**).**

3.3. *The effect of the surface on adenovirus physical properties*

We have evaluated how the physical and mechanical properties of virus particles vary according to the different adsorption interactions with the surfaces (TIPT+OCTS, HOPG and mica). In particular, we focused on the height, yield force and the elastic constant.

We studied the effect of the surface nature on the mechanical and physical properties of Ad5 and reovirus particles (Fig. S6**)**. We first focused on the characterization of the height and mechanical properties of Ad5 on hydrophobic surfaces and then on mica. To analyze mechanical properties, we performed nanoindentation tests.Fig. 2A shows a topography image of a single adenovirus particle adsorbed on TIPT+OCTS before indentation. The probed particle undergoes an elastic deformation upon tip contact, displayed in the curve as an initial linear range (red line, Fig. 2C**).** From the slope of the linear region of the curve we obtain information about the elasticity (stiffness) of the particles. After a certain force, the viral particle fails and loses its structural integrity (Fig. 2B), identified through a sudden drop in the force-indentation curve. The drop provides information about the deformation before failure (critical indentation) and the normal force applied before the structure yields (yield force). Both values are related to the brittleness of the particle. Profiles from topography images taken before and after the nanoindentation show the changes in particle height upon mechanical disruption (Fig. 2D). This process is repeated for several adenovirus particles on HOPG and TIPT+OCTS, (Fig. S8).

Fig. 3 shows the values of the average height and mechanical properties of Ad5 on the different surfaces. For functionalized surfaces (TIPT+OCTS), the average height of the virus is 90.2 ± 0.3 nm (N = 148) with respect to HOPG, 86.3 ± 0.5 nm (N = 148) **(**Fig. 3D and Table S1), indicating a stronger interaction with the substrate and higher deformability of the adsorbed particles on HOPG. Ad5 has an icosahedral capsid and can therefore adsorb on any of its three symmetry axes: 2-fold, 3-fold, and 5-fold. We cannot rule out that there is a preferential orientation on the HOPG surface. Fig. 3A,B,C and Fig S9A,B, C shows a comparison of the indentation curves obtained on the different surfaces, from which the respective mechanical properties of Ad5 have been obtained.

A comparison of the yield force on both surfaces shows that the force required to disrupt adenovirus particles is similar for TIPT+OCTS (4.7 ± 0.5 nN, N = 17, *mean* ± *SEM*) and for HOPG (3.6 ± 0.3 nN, N = 21) (Fig. 3E**).** One-way ANOVA test indicated that population means are not significantly different**.** Additionally, the elastic constant of the virus adsorbed on TIPT+OCTS (0.45 ± 0.04 N/m, N = 17) is similar to what determined on HOPG (0.42 ± 0.05 N/m, N = 21). One-way ANOVA test at 0.05 level indicated that population means are once more not significantly different (Fig. 3F**).** On the other hand, the average deformation of the capsid during the indentation experiments is 12.5 ± 1.4 nm (N = 17) for virus on TIPT+OCTS surfaces, and 10.0 ± 0.8 nm

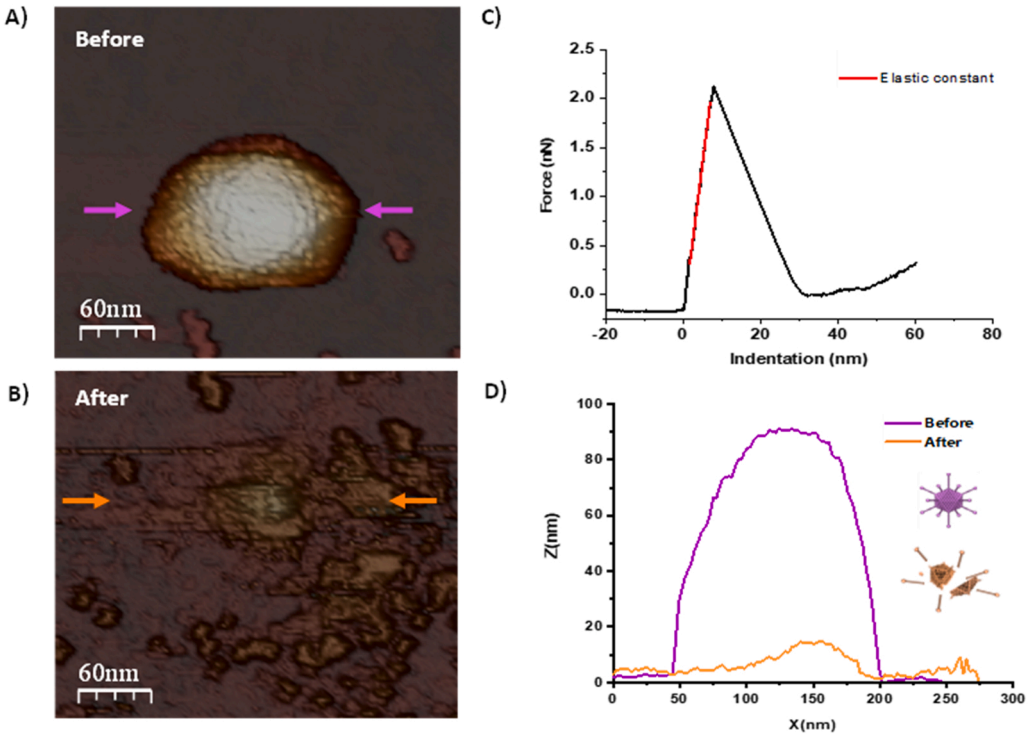

Fig. 2. AFM characterization of adenovirus on TIPT+OCTS: A) Image of the virus particle before indentation. B) Image of the virus particle after indentation. C) Indentation curve. The red line marks the slope of the curve that corresponds to the elastic constant value. D) Height profiles before and after indentation, taken along the lines indicated by arrows in (A) and (B).

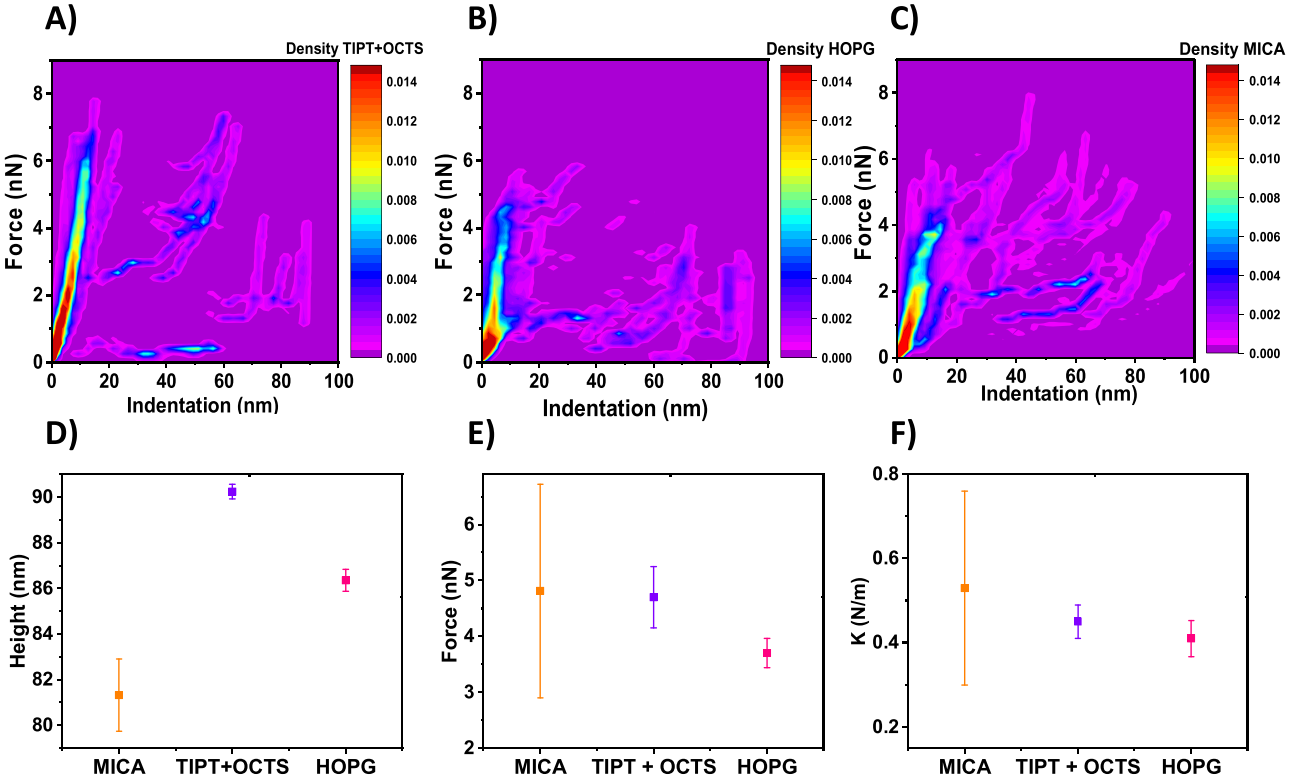

Fig. 3. Mechanical characterization of adenovirus. A), B) and C) Heat maps of the indentation curves for adenovirus on TIPT+OCTS, HOPG and mica respectively. D), E) and F) Comparison of the height, yield force and elastic constant value (mean ± standard error) for mica (orange), (TIPT+OCTS (purple) and HOPG (pink)).

(N = 21) for virus on HOPG surfaces. The ratio between the deformation and the height of the virus particle provides information about the critical deformation of the capsid. Critical strain refers to the maximum deformation undergone before failure, relative to the capsid outer diameter (Critical strain = critical indentation / particle height). The critical strain for Ad5 particles is 0.13 ± 0.01 on TIPT+OCTS and 0.11 ± 0.01 on HOPG.

On mica, a hydrophilic surface, Ad5 is absorbed by adding nickel chloride to the buffer. On this surface Ad5 particles present a height of 83 ± 2 nm (N = 55), which suggests higher deformation on this surface or a different adsorption symmetry, comparing with hydrophobic surfaces (HOPG and TIPT+OCTS) (Fig. 3D). On the other hand, the yield force on mica (4.7 ± 0.3 nN, N = 33) is comparable to that on TIPT+OCTS (Fig. 3C,E). The value of elastic constant of particles adsorbed on mica surface is 0.56 ± 0.05 N/m (N = 33) (Fig. 3F). The values of the deformation on mica (12.1 ± 0.7 nm, (N = 31)) and the critical strain (0.14 ± 0.01 (N = 31)) are comparable to those obtained on TIPT+OCTS. The mechanical properties of Ad5 adsorption on mica reported in the literature, previously [45,58] were 88 ± 2 nm (N = 97) for the height, 5.0 ± 0.1 nN (N = 77) for the yield force and 0.56 ± 0.02 N/m (N = 77) for the elastic constant. These values indicate that our results are in agreement with previously reported results by A. Ortega-Esteban et.al [12,49,58], which supports the validity of our experimental data and procedure.

3.4. The effect of the surface on reovirus properties

We have investigated the mechanical properties of reovirus particles on TIPT+OCTS and HOPG surfaces. Experiments with reovirus were carried out using the same protocols as for adenovirus. Reovirus particles were imaged before and after indentation (Fig. 4 and Fig. S10). The height of the reovirus particles was 73 ± 2 nm (N = 14) on TIPT+OCTS and 75 ± 2 nm (N = 12) on HOPG, indicating that their height remains unaltered independently of the surface nature (Fig. S11C and Table S1).

Statistical analysis performed of the yield force on both surfaces (Fig. 5A,B, and Fig. S11A,B) reveals that the substrate is significantly affecting : 4.0 ± 0.3 nN (N = 14) and 3.0 ± 0.4nN (N = 13) for the TIPT+OCTS and HOPG respectively, (One-way ANOVA, $p < 0.05$, indicated that population means are significantly different) (Fig. 5D) Also, there are noticeable differences in the elastic constant (Fig. 5E). The elasticity of the viruses is significantly lower ($p < 0.05$) for TIPT+OCTS surfaces 0.6 ± 0.1 N/m (N = 13) in contrast to HOPG (0.3 ± 0.1 N/m, N = 12).

The values of the deformation produced by the indentation are 7.5 ± 1.8 nm (N = 13) for TIPT+OCTS surfaces and 12.3 ± 1.7 nm (N = 11) for HOPG surfaces. Also, the values of the critical strain are 0.10 ± 0.02 (N = 13) for TIPT+OCTS and 0.16 ± 0.01 (N = 11) for HOPG, indicating that on TIPT+OCTS the viruses are less elastic than on HOPG (Fig. S11).

4. Discussion and conclusions

In this work we have demonstrated that the nature of the substrate surface influences the interactions with the virus capsids varying the affinity and could play a key role in the determination of the mechanical properties of the capsid of some viruses.

The Sol-Gel method has allowed us to integrate alkane queues in TIPT films as shown by FTIR. The band present at circa 3000 cm^{-1} in the spectrum of TIPT is a clear fingerprint of alkane integration, in contrast

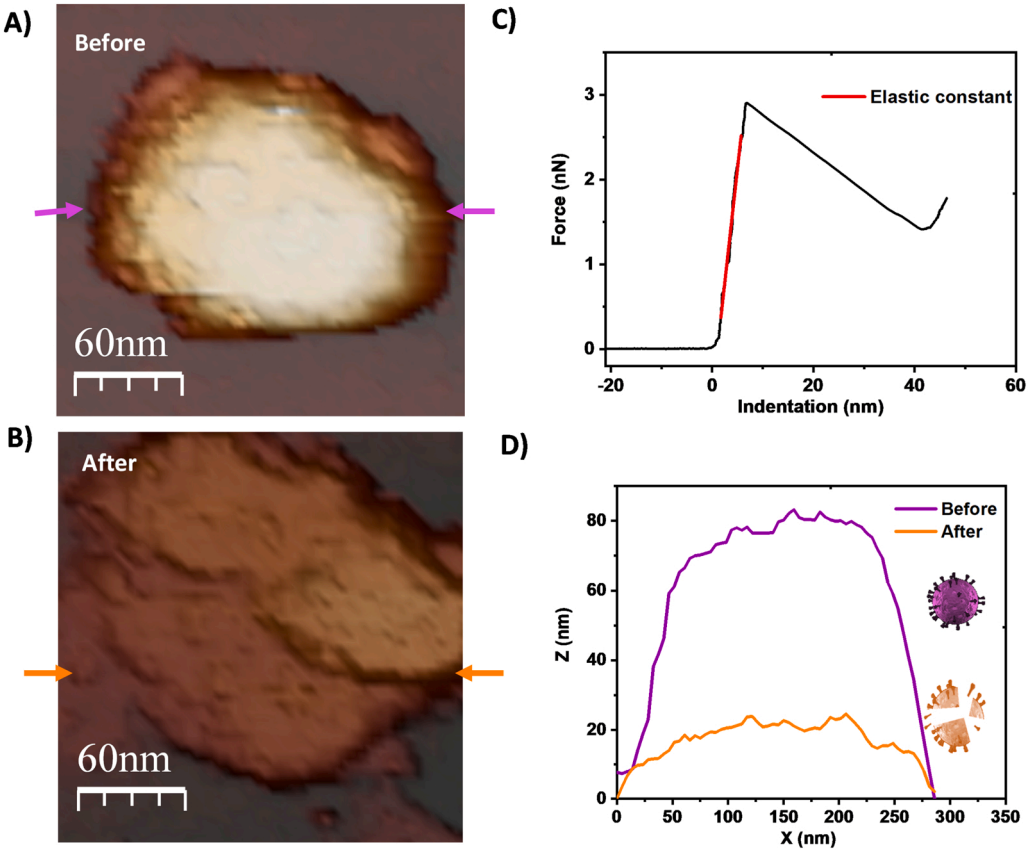

Fig. 4. : AFM characterization of the reovirus on TIPT+OCTS: reovirus adsorbed on TIPT+OCTS. A) Image of the virus before indentation. The arrows mark the height profile line. B) Image of the virus after indentation. C) Indentation curve. The red line marks the slope of the curve that corresponds to the elastic constant value. D) Virus height profiles before and after indentation.

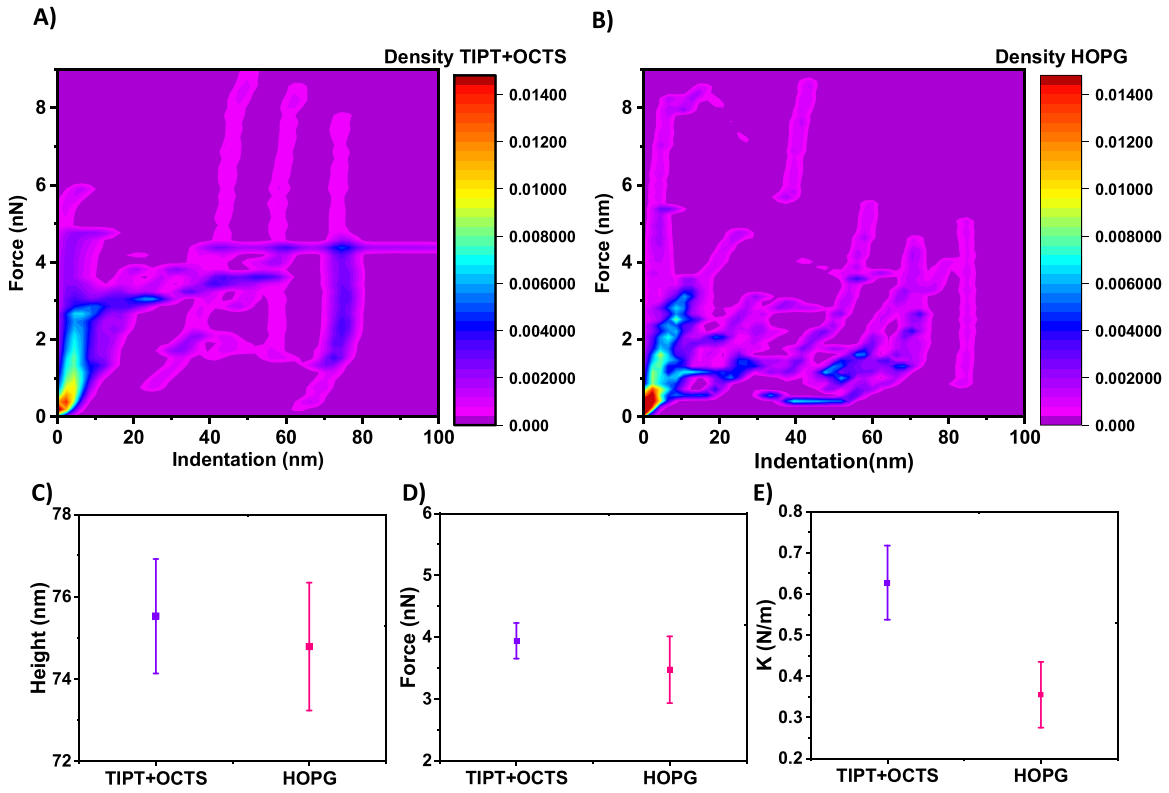

Fig. 5. Mechanical characterization of reovirus: A) and B) Heat maps of the indentation curves for reovirus on TIPT+OCTS and HOPG, respectively. C), D) and F) Plots comparing height, yield force and elastic constant values (mean ± standard error) on the different surfaces (TIPT+OCTS (purple) HOPG (pink)).

with characteristic groups of different silane compounds [57]. In the RBS spectra, we could confirm that the main difference between the pure TIPT and the TIPT+OCTS film is the presence of a C-rich and Si decorated surface on the OCTS functionalized film. The presence of a Si 2p core level contribution in the XPS spectrum of the OCTS functionalized surface confirms the successful funcionalization. Also, the ratio between the C-O and C-H contributions, which presents a lower value in the case of surfaces containing OCTS, further suggests the presence of an alkane enriched surface on OCTS functionalized surfaces.

Surfaces of TIPT+OCTS with 0.1 M OCTS content, and subjected to soft annealing, allow maximizing the hydrophobic behavior in compatibility with low roughness, as verified by AFM analysis. The combination of surface hydrophobicity and homogeneity has been exploited for the topographic and mechanical analysis of viral particles. Moreover, the number of viral particles adsorbed on the surface increases with the hydrophobic character of the surface. In particular, the number of particles adsorbed is higher on TIPT+OCTS with respect to HOPG, suggesting an increase in the physisorption of viruses in comparison with the standard hydrophobic surfaces used for virus characterization. In terms of thermodynamic models, this suggests that future work should be devoted to estimate the Flory-Huggins interaction parameter, which may provide valuable information on the adhesive regime and stability [59] of the adsorbed viral capsids.

In the mechanical analysis of Ad5, we have observed less deformed particles in the adsorption process on TIPT+OCTS surfaces. Moreover, the adenovirus particles adsorbed on mica in presence of nickel chloride present similar values of the yield force and elasticity in comparison with hydrophobic surfaces, which is in agreement with values previously reported in literature [60,61]. This sets an internal control for the measurements performed in our experiments and provide confidence on our experimental data and procedure. In another work, the authors characterized the mechanical properties of Ad35F (Ad5 pseudotyped with the Ad35 fiber) on hexamethyldisilazane (HMDS) functionalized surfaces, where they observed a dependency between the elastic response and the displayed symmetry of the attached particles [62]. The values obtained for the elastic constant were 1.03 ± 0.08 N/m (N = 5); 0.41 ± 0.02 N/m (N = 8); 0.29 ± 0.04 N/m (N = 10) for the case of S2, S3 and S5 symmetries, respectively. The value of the elastic constant that most closely resembles our values on the TIPT+OCTS surface is the one corresponding to the S3 symmetry. The values reported for the yield force were: 4.5 ± 0.2 nN (N = 5); 4.2 ± 0.3 nN (N = 8); and 2.0 ± 0.4 nN (N = 10) for the case of S2, S3 and S5 symmetry axes respectively [45]. The S2 and S3 symmetries display similar and comparable values to our estimates of mechanical properties. Although the measurements were not related to specific symmetries, previous studies suggest that the most probable adsorption symmetry is S3 [60]. Therefore, it would be interesting for the future to characterize the adsorption symmetry of the viral particles and assign the specific mechanical properties to each symmetry axis. A study of the effect of the nickel chloride on the capsid structure would also be convenient.

In the literature there are other reported examples where the mechanical response of the viruses does not vary with the substrate nature when carrying out nanoindentation studies. For example, in the case of bacteriophage Ø29, one of the smallest known dsDNA-containing phages [63]. Studies of the mechanical characteristics of the prohead have been carried out on silanized glass and HOPG. Prohead adsorbed on silanized glass surface, reached elastic constant of 0.192 ± 0.034 N/m [64], which is very close to the value obtained for the prohead adsorbed on HOPG (0.23 ± 0.05 N/m) [39].

This same trend has also been observed on Minute Virus of Mice (MVM), a small non-enveloped virus with a single-stranded DNA genome. The mechanical properties of this virus have been studied on silanized glass surface and on HOPG. The elastic constant on the silanized glass surface is 0.5 ± 0.2 N/m for S5 symmetry and 0.84 ± 0.12 N/m for S3 symmetry [65]. For the case of HOPG, the value of the elastic constant is 0.6 N/m for S5 symmetry and 0.8 N/m for S3 symmetry [66]. Therefore, the obtained elastic constant values do not vary significantly in this case when the virus is attached on different hydrophobic surfaces.

Also, a recent study has shown that the small deformation suffered by the capsids when adsorbing on the surface does not affect the measured mechanical response [67]. The results show that the TIPT+OCTS surfaces increase the reliability of the mechanical tests on virus capsids by, on the one hand, reducing the dispersion of data obtained on adenovirus.

On the other hand, reovirus has been mechanically described for the first time. TIPT+OCTS surfaces do not cause a great difference in the deformation of the reovirus particles upon deposition. Moreover, the reovirus particles exhibit an increase in stiffness and yield force compared to those adsorbed on HOPG, but no changes in the critical strain. This result suggests that the differences in elasticity could have origin in the virus structure (double shell of proteins and a genome comprised of double-stranded RNA).

Our results indicate that TIPT+OCTS surfaces behave, on the one hand, as more efficient hydrophobic sorptive surfaces of viral particles than standard Mica and HOPG, and, on the other hand, behave as analogue to the former surfaces for the determination of height, yield force and elastic modulus of the viral particles. In overall, they offer a statistical gain for the mechanical analysis of viral capsids, which could be extended specially to viral particles of biotechnological interest.

CRediT authorship contribution statement

A.S.C: AFM experiments, surfaces preparation, surfaces characterization, AFM data analysis, Writing - original draft. M.C: AFM experiments, input in the Writing - original draft. U.P: adenovirus purification. P.O-G: reovirus purification. C.S.M: contributed reagents, input in the Writing - original draft. P.J.P: Input in the writing - original draft, contributed analysis and experimental tools. M.M.S: designed the research, supervising surfaces preparation and characterization. M.H-P: designed the research, AFM experiments, supervising AFM data analysis. M.M.S and M.H-P: wrote the paper with input from all other authors.

Declaration of Competing Interest

The authors declare that they have no known competing financial interests or personal relationships that could have appeared to influence the work reported in this paper.

Data availability

Data will be made available on request.

Acknowledgments

We acknowledge Dr. Cristina Risco (CNB-CSIC) for insightful and motivation discussion. This work was supported by the grant Ayudas a Proyectos de I+D para Jóvenes Doctores de la Universidad Autónoma de Madrid 2021 (SI3/PJI/2021–00216) supported by Comunidad de Madrid and Universidad Autónoma de Madrid to M.H-P. Also, M.H-P acknowledges funding from the Spanish Ministry of Science and Innovation (TED2021–129937B-I00). Grant PID2019–104098GB-I00/AEI/10.13039/501100011033, co-funded by the Spanish State Research Agency and the European Regional Development Fund to C.S.M. The CNB-CSIC was further supported by a Spanish State Research Agency Severo Ochoa Excellence grant (SEV 2017–0712). C.S.M is a member of the CSIC funded consortium LifeHub (CSIC grant number: 202120E47). REACT-EU funding by Comunidad Autónoma de Madrid is also acknowledged. M.M.S acknowledges funding from MCIN/AEI/10.13039/501100011033 (PID2020–112770RB-C22). P.J.P acknowledges projects FIS2017–89549-R; and FIS2017–90701-REDT. P.J.P also acknowledges the Human Frontiers Science Program (HFSPO RGP0012/2018).

Appendix A. Supporting information

Supplementary data associated with this article can be found in the online version at doi:10.1016/j.colsurfb.2023.113136.

References

[1] J. Louten, Essent. Hum. Virol. (2016) 19–29.
[2] A.V.S. Hill, et al., Cancer Immunol Res 9 (2021) IA11.
[3] L. Jiménez-Cabello, et al., Microorganisms 9 (2021) 42.
[4] L.A. Lee, et al., Nanomedicine 2 (2006) 137–149.
[5] E. Sokullu, et al., Pharmaceutics 11 (2019) 211.
[6] H. Bar, et al., BMC Biotechnol. volume, 8 (2008) 37.
[7] Douglas Trevor, et al., Science 12 (312) (2006) 873–875.
[8] M. Young, et al., Annu Rev. Phytopathol. 46 (2008) 361–384.
[9] C. Varanda, et al., Viruses 13 (2021) 2073.
[10] L.A. Colnago, et al., Int. J. Environ. Res. Public Health 17 (2020) 6456.
[11] J. Katainen, et al., J. Colloid Interface Sci. 304 (2006) 524–529.
[12] A. Ortega-Esteban, et al., Sci. Rep. 3 (2013) 1434.
[13] P.J. De Pablo, et al., J. Adhes. 71 (1999) 339–356.
[14] K.L. Johnson, et al., Proc. R. Soc. Lond. 324 (1971) 301–313.
[15] M. Calleja, et al., J. Appl. Phys. 92 (2002) 5539.
[16] J.F.L. Duval, et al., Langmuir 20 (2004) 5052–5065.
[17] C.P. Gerba, Adv. Appl. Microbiol. 30 (1984) 133–168.
[18] D. Tabor, J. Colloid Interface Sci. 58 (1977) 2–13.
[19] D. Moreno-Cerrada, et al., Biointerphases 14 (2019), 011001.
[20] D. Rana, et al., Macromolecules 29 (1996) 1579–1583.
[21] S.S. Datta, et al., Proc. Natl. Acad. Sci. 113 (2016) 7041–7046.
[22] L.D. Soule, et al., ACS Biomater. Sci. Eng. 6 (2020) 5549–5562.
[23] M. Manso-Silván, et al., Biomed. Micro 9 (2007) 287–294.
[24] J.M. Moreno, et al., Surfaces 3 (2020) 352–365.
[25] C. San Martín, Viruses 4 (2012) 847–877.
[26] K. Kosulin, Viruses 11 (2019) 804.
[27] W. Wold, et al., Curr. Gene Ther. 13 (2013) 421–433.
[28] F. Sakurai, et al., Drug Metab. Pharm. (2021), 100432.
[29] H. Kaufman, et al., Nat. Rev. Drug Disco 9 (2015) 642–662.
[30] P.J. de Pablo, et al., Phys. Rev. Lett. (2003) 91–99.
[31] C. Comins, et al., Clin. Oncol. (R. Coll. Radio.) 20 (2008) 548–554.
[32] R. Bouziat, et al., Science 356 (2017) 44–50.
[33] C. Comins, et al., Gene Therapy of Cancer, Third edition, Chapter 13, Academic Press, 2014, pp. 185–198.
[34] O. Baranov, et al., J. Russ. Chem. Bull. 69 (2020) 1165–1168.
[35] M. Brehm, et al., Adv. Mater. Interfaces 7 (2020).
[36] I.A. Fornazari, et al., Oper. Dent. 42 (2017) 367–374.
[37] M. Hernando-Pérez, et al., ACS Nano 13 (2019) 7842–7849.
[38] P.J. de Pablo, Subcell Biochem. 68 (2013) 247–271.
[39] M. Hernando-Pérez, et al., Small 8 (2012) 2366–2370.
[40] M. Hernando-Pérez, et al., Nat. Commun. 5 (2014) 4520.
[41] M. Mayer, Proceedings of the 15th International Conference on the Application of Accelerators in Research and Industry, Am. Inst. Phys. Conf. Proc. (1999).
[42] R. Alba, et al., Virology 367 (2007) 51–58.
[43] D.B. Furlong, et al., J. Virol. 62 (1988) 246–256.
[44] R.E. Smith, et al., Virology 39 (1969) 791–810.
[45] J. Snijder, et al., J. Virol. 87 (2013) 2756–2766.
[46] F. Moreno-Madrid, et al. 45 (2017) 499–511.
[47] P.J. de Pablo, et al., Adv. Exp. Med. Biol. 1215 (2019) 159–179.
[48] M. Hernando-Pérez, et al., Nanoscale 7 (2015) 17289–17298.
[49] A. Ortega-Esteban, et al., ACS Nano 9 (2015) 10826–10833.
[50] A. Ortega-Esteban, et al., Ultramicroscopy 114 (2012) 56–61.
[51] I. Horcas, et al., Rev. Sci. Instrum. 78 (2007) 13705.
[52] M. Kopani, et al., MRS Proc. 1066 (2008), 10660703.
[53] N.A. Lapin, et al., J. Phys. Chem. B 113 (2009) 8776–8783.
[54] A. Muñoz-Noval, et al., Langmuir 28 (2012) 1909–1913.
[55] A. Kozbial, et al., Langmuir 30 (2014) 8598–8606.
[56] S. Chattopadhyay, et al., Environ. Sci. Technol. 33 (1999) 3609–3614.
[57] A. Armanious, et al., Environ. Sci. Technol. 50 (2016) 732–743.
[58] A. Ortega-Esteban, et al., Methods Mol. Biol. 1886 (2019) 259–278.
[59] M. Khayet, et al., J. Membr. Sci. 263 (2005) 77–95.
[60] A. Ortega, Thesis (2015).
[61] M. Pérez-Illana, et al., Acta Biomater. 135 (2021) 534–542.
[62] J.R. Snijder, et al., J. Virol. 87 (2013) 2756–2766.
[63] W.J.J. Meijer, et al., Microbiol. Mol. Biol. Rev. 65 (2001) 261.
[64] C. Carrasco, et al., Biophys. J. 100 (2011) 1100–1108.
[65] C. Carrasco, et al., Proc. Natl. Acad. Sci. USA 105 (2008) 4150–4155.
[66] D. Matínez-Martín, et al., Plos One 7 (2012), e30204.
[67] C. Zeng, et al., Phys. Rev. Lett. 119 (2017), 038102.